

Eruption Source Parameters for forecasting ash dispersion and deposition from vulcanian eruptions at Tungurahua volcano: Insights from field data from the July 2013 eruption



René Parra ^{a,*}, Benjamin Bernard ^{a,b}, Diego Narváez ^b, Jean-Luc Le Pennec ^c, Nathalie Hasselle ^d, Arnau Folch ^e

^a Universidad San Francisco de Quito, Colegio de Ciencias e Ingeniería, Diego de Robles y Vía Interoceánica, Quito, Ecuador

^b Instituto Geofísico, Escuela Politécnica Nacional, Ladrón de Guevara E11-253, Ap 17-2759 Quito, Ecuador

^c Laboratoire Magmas et Volcans (LMV), Université Blaise Pascal, Clermont-Ferrand, France

^d Laboratoire de Volcanologie, Université Libre de Bruxelles, Belgium

^e Barcelona Supercomputing Center, Centro Nacional de Supercomputación (BSC-CNS), Barcelona, Spain

ARTICLE INFO

Article history:

Received 17 April 2015

Accepted 2 November 2015

Available online 10 November 2015

Keywords:

Volcanic ash

ESP

Vulcanian eruptions

WRF

FALL3D

Tungurahua

ABSTRACT

Tungurahua volcano, located in the central area of the Ecuadorian Sierra, is erupting intermittently since 1999 alternating between periods of quiescence and explosive activity. Volcanic ash has been the most frequent and widespread hazard provoking air contamination episodes and impacts on human health, animals and crops in the surrounding area. After two months of quiescence, Tungurahua erupted violently on 14th July 2013 generating short-lived eruptive columns rising up to 9 km above the vent characterized as a vulcanian eruption. The resulting fallout deposits were sampled daily during and after the eruptions to determine grain size distributions and perform morphological and componentry analyses. Dispersion and sedimentation of ash were simulated numerically coupling the meteorological Weather Research Forecasting (WRF) with the volcanic ash dispersion FALL3D models. The combination of field and numerical studies allowed constraining the Eruption Source Parameters (ESP) for this event, which could be used to forecast ash dispersion and deposition from future vulcanian eruptions at Tungurahua. This set of pre-defined ESP was further validated using two different eruptions, as blind test, occurring on 16th December 2012 and 1st February 2014.

© 2015 Elsevier B.V. All rights reserved.

1. Introduction

The Ecuadorian volcanic arc hosts about 85 quaternary volcanoes, 25 of which are erupting, active or potentially active (Fig. 1). In the last 15 years, 4 volcanoes produced moderate to large explosive eruptions with significant ash plumes (Pichincha 1999–2001, Sangay permanent, Tungurahua 1999 to present, El Reventador 2002 to present). These eruptions caused ash fallout leading to disruptions of Quito and Guayaquil international airports and affected large areas, provoking health issues and damaging crops and infrastructures (Le Pennec et al., 2012). Tungurahua (Lat. 01° 28' S; Lon. 78° 27' W; 5023 m asl) is a large stratovolcano located in the Real Cordillera of the Ecuadorian Andes (Hall et al., 1999). Since the beginning of its current activity in October 1999, ash fallout has been the most frequent and widespread volcanic hazard (Le Pennec et al., 2012; Bernard et al., 2013a; Eychenne et al., 2013). During this period, Tungurahua has alternated between quiescence periods and eruptive phases. Until 2009 each reawakening was progressive, but the behavior varied since May 2010, with activity

starting only a few days or hours before a paroxysmal event (Hidalgo et al., 2015). Based on seismic–acoustic signals, some of the current explosive onsets have been characterized as vulcanian (Kim et al., 2014).

Volcanic ash can cause critical air pollution events with significant environmental impacts (Ayris and Delmelle, 2012). Associated hazards are varied and can include damage to buildings, road traffic accidents due to reduction of visibility, health issues brought on by inhalation of fine particulates and irritation of mucosae, and disruptions of air traffic on a larger scale (Horwell and Baxter, 2006; Wilson and Stewart, 2012). To protect public health and improve risk management, regions potentially affected should rely on information regarding the possible ash dispersion trajectories and ground deposition patterns (e.g. Macedonio et al., 2005; Bonasia et al., 2014). In this sense, atmospheric dispersion models are pivotal for forecasting ash deposition at regions under the influence of active volcanoes (e.g. Folch et al., 2008; Scollo et al., 2009; Collini et al., 2013; Wilkins et al., 2014). These models require meteorological forecasts and a set of volcanological inputs, the Eruption Source Parameters (ESP) (Bonadonna et al., 2011), including particle grain size distribution and the characterization of the source term (i.e., eruption duration, plume height, mass eruption rate and vertical distribution of mass along the eruptive column). Based on a compilation

* Corresponding author. Tel.: +593 22890070x1209.
E-mail address: rparra@usfq.edu.ec (R. Parra).

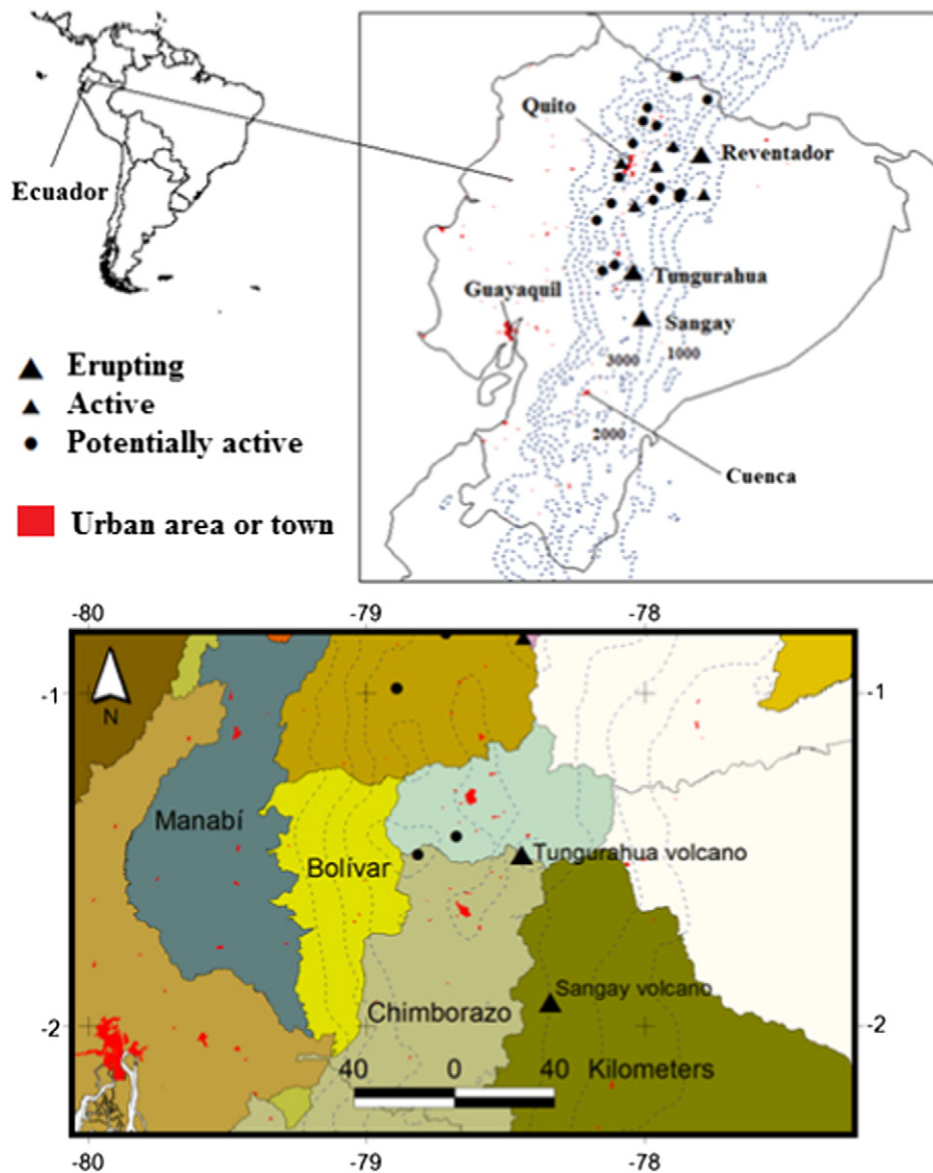


Fig. 1. Erupting, active and potentially active volcanoes in Ecuador. Dashed lines depict topography in m asl.

of published data, Mastin et al. (2009a) proposed a preliminary spread sheet of ESP for different types of eruptions. This a priori set of inputs has the advantage that the ESP can be used as an initial guess for running pre-eruptive forecasts (or even syn-eruptive forecasts in case of remote, unmonitored volcanoes or simply whenever updated observations are not available on time). The strategy is particularly useful for volcanoes poorly studied or having an insufficient eruptive record. However, it is clear that disposing of dedicated ESP for a given volcano is a preferable option. This is particularly critical in case of short-living (eg. vulcanian) eruptions, for which it is very difficult to assimilate observations (i.e. to update pre-defined ESP) and then run a forecast before tephra fallout actually affects the proximal locations. This paper aims to define a set of ESP for vulcanian activity at Tungurahua volcano. For this purpose, we combine field and laboratory studies with numerical simulations of the 14th July 2013 eruption. The obtained set of ESP is then validated by modeling two different eruptions emulating an operational forecast. The ultimate goal is to improve the forecasts of volcanic ash dispersal and fallout, a key objective of the Research Group of Volcanic Ash in Ecuador (“Grupo de Investigación sobre la Ceniza Volcánica en el Ecuador”, GICVE).

2. July 2013 eruption

After two months of superficial quiescence and weak fumarolic activity, Tungurahua volcano produced a large explosion on 14th July 2013 at 06:47 LT (LT = UTC – 5 h). The explosion was followed by a tremor that lasted until 08:40 LT according to the Instituto Geofísico de la Escuela Politécnica Nacional (IGEPN, 2013a). In terms of seismic and acoustic amplitudes and energies, the first explosion was the largest explosion recorded at Tungurahua since the beginning of extensive monitoring in July 2006 (A. Steele, personal communication). The explosion was heard in the city of Guayaquil, at a distance of about 180 km away from (IGEPN, 2013a). Heavy tephra fallout was reported at the W of the volcano, in the localities of Bilbao, Chacauco, Cotalo, Cahujá, Choglontus, El Manzano, Puela and Penipe (IGEPN, 2013b). Ash fallout affected also more distant villages and towns across the provinces of Chimborazo, Tungurahua, Bolivar, and Manabí. The eruption also produced large ballistic projectiles, with impact craters observed on the N flank up to 4.3 km from the vent. Shortly after the initial large explosion, pyroclastic density currents (PDCs) flowed in at least nine drainages on the N, NW and W flanks of the volcano, reaching

a maximum distance of 7.5 km from the crater. The eruptive activity continued with variable intensity and sporadic ash fallout until the 2nd of August. Based on these characteristics we classified the eruption of the 14th July 2013 as vulcanian (Self et al., 1979); which is consistent with the current seismic–acoustic characterization made by Kim et al. (2014).

2.1. Ash sampling and deposit data

As of December 2010, Tungurahua is equipped with a monitoring network that collects daily data of fallout during eruptive periods (Bernard et al., 2012). Volunteers living in four localities around the volcano (Choglontus, Pillate, Palictahua and Runtun; see Fig. 2) participate in the collection of data. The network has homemade ashmeters (Bernard, 2013) and electronic scales. Sampling is routinely performed weekly when there is no eruption, and daily during eruptive events. This strategy provides high temporal resolution data and avoids data misrepresentation by contamination and/or reworking of fresh deposits. The team of volunteers weighs the samples with a 0.1 g portable scale, then seals and labels them in plastic bags. Once in the laboratory,

samples are dried at 40 °C during 24 h and weighed on a 0.01 g precision scale. The result is an excellent high-density deposit load dataset with a resolution < 10 g/m² measured in the field and < 1 g/m² in laboratory. At the end of each eruption, volcanologists make a global survey to complement the daily dataset. This final survey includes an extensive network of ashmeters that covers a large part of Tungurahua and Chimborazo provinces (Bernard et al., 2013b). The information is used to create isomass maps of the fallout deposit and to calculate the total erupted mass by means of different approaches (Pyle, 1989; Fierstein and Nathenson, 1992; Legros, 2000; Bonadonna and Houghton, 2005; Bonadonna and Costa, 2012). By comparing the daily measurements (available only at four locations) and the global survey, the amount of ash deposited daily can be extrapolated across the whole deposit.

The July 2013 eruption affected mainly the areas of Choglontus and Pillate, with a total measured accumulation of 3037 g/m² and 633 g/m² respectively. These values are consistent with the global survey made at the end of the eruption (3025 g/m² at Choglontus and 623 g/m² at Pillate), highlighting the reliability of the daily volunteer sampling. The fallout recorded at Choglontus (1206 g/m²) and Pillate (304 g/m²) during 14th July represents 40% and 48% respectively of

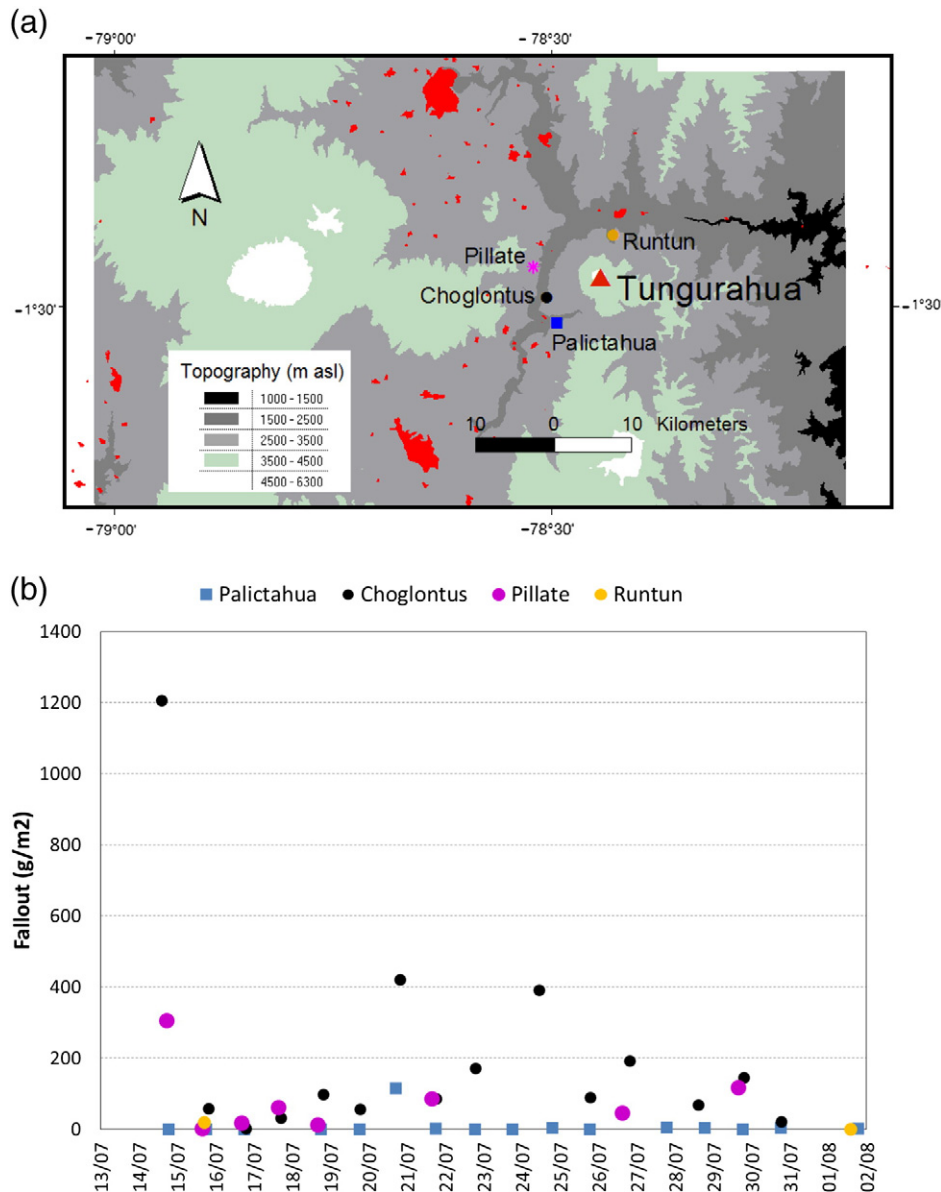


Fig. 2. Location of the volunteer network around Tungurahua volcano (a) and dry area-densities for the daily ash fall recorded by the network during the July 2013 eruption (b).

the total deposit at these two stations. In contrast, the localities of Palictahua and Runtun were almost unaffected by fallout from this event because the wind direction during that day was towards WSW.

During the global survey performed from 15th to 17th August 2013, 51 ash samples were collected. However, reliable thickness reading was possible only in 17 locations due to the threshold of the ashmeter (0.3 mm). This number of samples is too low to draw an isopach map with good confidence, but allows calculating bulk densities of the fallout deposit. The compilation of the area density (ground load) permitted to draw an isomass map with 9 isomass curves (Fig. 3). The sinuous shape of the isomass curves probably reflects the topographic effects of the Igualata volcano (located at the WSW of Tungurahua) on the local wind field. The plot of area density versus square root of isomass area was used to calculate the total mass deposited during the July 2013 eruption using 6 different methods (Table 1). Amongst these, the Power Law method was discarded because the low exponent obtained (1.083) implies a large uncertainty in the results (Bonadonna and Houghton, 2005). The other 5 methods gave quite consistent results, with erupted mass ranging between 6.26 and 7.2×10^8 kg.

3. Fallout quantification and Eruption Source Parameters (ESP)

3.1. Total Grain Size Distribution (TGSD)

Samples from the daily and global surveys allow determining the grain size distribution (GSD), componentry and particle morphology. For the 14th July paroxysm only the Choglontus sample could be considered for two reasons: 1) the volcanic plume was over Choglontus area for most of the eruption and, 2) the Choglontus sample was the only one large enough to perform grain size analysis by sieving. The GSD was determined through manual sieving from 2 mm to $45 \mu\text{m}$ (-1ϕ to 4.5ϕ at 0.5ϕ intervals) in the Universidad San Francisco de Quito (USFQ) laboratory. For the whole July fallout the GSDs were determined through manual sieving from 16 mm to $32 \mu\text{m}$ (-4ϕ to 5ϕ at 0.5ϕ intervals).

Due to the limited information available, it is not possible to reconstruct the TGSD for the 14th July event. However, it is possible to combine the information from the Choglontus station with the global survey to estimate this parameter (Table 2). The sample collected by the Choglontus volunteer after the 14th July eruption shows a clear bimodal GSD (Fig. 4, Table 2). Deconvolution of the Gaussian mixture using the program SFT (Wohletz et al., 1989) gives a principal mode at 0.41ϕ that represents 67% of the sample and a secondary mode at 3.73ϕ that represents 30% of the sample (a similar bimodal GSD was documented by Eychenne et al. (2012) for the deposits of the 16th

Table 1

Total deposit mass of the July 2013 Tungurahua eruption calculated with 6 different methods. The Power Law method is discarded because of the very low exponent of the power law. R^2 is excellent (>0.99) for all the methods except for the Power Law.

Method	Reference	Remark	R^2	Total mass ($\times 10^8$ kg)
1 isomass	Legros (2000)	0.8 kg m^{-2} isomass		6.54
1 segment	Pyle (1989)		0.998	6.47
2 segments	Fierstein and Nathenson (1992)	Segment 1	0.998	7.20
		Segment 2	0.999	
3 segments	Bonadonna and Houghton (2005)	Segment 1	0.999	7.16
		Segment 2	1.000	
		Segment 3	0.999	
Weibull	Bonadonna and Costa (2012)		0.998	6.26
Power Law	Bonadonna and Houghton (2005)	Discarded ($m = 1.083$)	0.979	
Average				6.72

August 2006 eruption). The coarse mode is interpreted as the product of the sedimentation from the eruptive plume while the fine mode probably corresponds to the ash cloud elutriated from the pyroclastic flow that descended from the Juive-La Pampa and Achupashal gullies. The sample contains 14 wt.% of fine ash ($<63 \mu\text{m}$; $>4\phi$), probably related to the abrasion of pyroclasts within the vent after fragmentation (Heiken and Wohletz, 1985) or in the pyroclastic flows (Kueppers et al., 2012).

Grain-size analyses (from -4 to 5ϕ) were performed on 29 samples from the global survey (Table 2). The area-weighted Total Grain Size Distribution (TGSD) was obtained using the Voronoi tessellation technique (Bonadonna and Houghton, 2005). The Choglontus sample and the TGSD for the entire July eruption show a similar trimodal GSD (Fig. 4, Table 2). The coarse and fine modes are very similar to the ones found in the 14th July sample, but an additional intermediate mode (not observed in the 14th July sample) appears around 2.5ϕ . Interestingly, the Choglontus samples from the 20th and the 24th of July (the other two days of the eruption with major ash fallouts) have a principal mode at around 2ϕ (Fig. 4, Table 2). Several other locations strongly affected by the 14th July fallout, such as Cahuaji and Jaloa la Playa, also present a trimodal distribution with a coarse mode between -1.21ϕ and 1.02ϕ , an intermediate mode between 2.07ϕ and 2.92ϕ , and a fine mode between 3.53ϕ and 4.27ϕ . At different locations, the coarse and intermediate modes clearly become finer away from the volcano or close to the edge of the plume, but the fine mode remains almost constant. Other sites that were not affected by the 14th July fallout (e.g. Palictahua or Matus Bajo) have a principal mode between 1.79

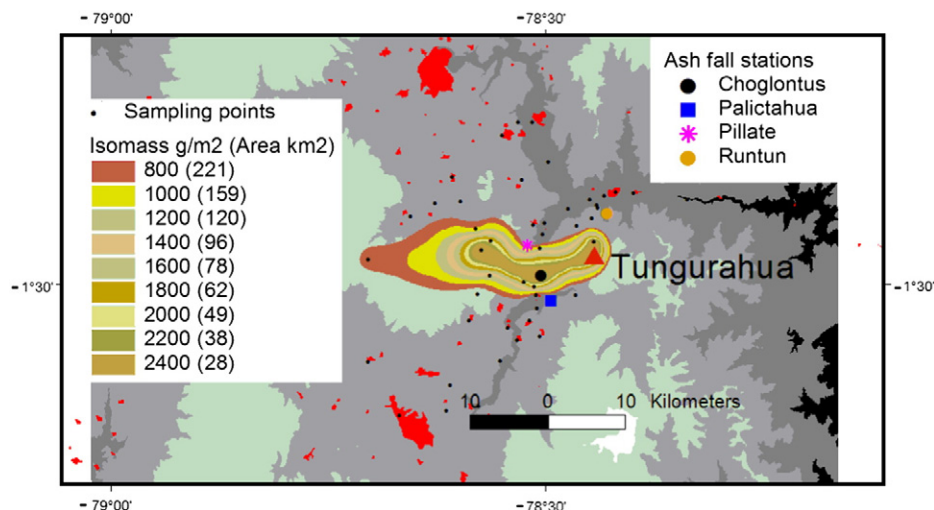


Fig. 3. Isomass map for the July 2013 tephra fallout.

Table 2

Graphical statistics and modes of the grain size analysis from the July 2013 Tungurahua eruption. Deconvolution of the Gaussian mixture was performed using the program SFT (Wohletz et al., 1989). All numbers apart from percentages are in ϕ unit. Md: median; Sigma-Phi: standard deviation; SkG: Skewness; Mz: mean; Sigma-I: inclusive standard deviation; SkI: inclusive skewness; KG: Kurtosis.

Sample site	Inman (1952) graphical statistics			Folk and Ward (1957) graphical statistics				Gaussian mixture deconvolution					
	Md	Sigma-Phi	SkG	Mz	Sigma-I	SkI	KG	Mode 1	Fraction M1	Mode 2	Fraction M2	Mode 3	Fraction M3
<i>Affected by the 14th July ashfall</i>													
Bilbao	1.8	2.58	−0.11	1.62	2.21	−0.08	0.6	−1.18	25%	1.79	51%	4.12	24%
Cahuaji	2.25	1.55	−0.03	2.22	1.44	−0.06	0.9	0.66	32%	2.36	46%	3.91	22%
Chacauco	2.55	2.3	−0.46	1.85	2.01	−0.4	0.58	−0.78	37%			3.32	61%
Chogllontus	2.3	1.83	−0.12	2.15	2.06	−0.29	1.29	0.54	24%	2.29	47%	3.99	30%
Chogllontus 14-07	0.85	1.93	0.48	1.47	1.73	0.38	0.66	0.41	67%			3.73	30%
Chontapamba	3.05	1.33	−0.36	2.73	1.37	−0.42	1.1	−0.4	11%	2.07	34%	3.53	55%
Chonturco	4.15	1.05	−0.48	3.82	1.34	−0.6	2.21	1.15	23%			4.34	77%
Cotalo	−1.05	0.93	−0.14	−1.13	0.9	−0.05	1.32	−1.02	94%				
Jalao la Playa	1.8	1.85	0.05	1.87	1.63	0.05	0.61	0.3	48%	2.6	27%	3.87	25%
Manzano	2.35	1.3	0.19	2.52	1.3	0.05	1.01	1.01	24%	2.22	50%	4.01	26%
Mocha	2.4	1.55	0	2.4	1.36	0.01	0.63	1.02	46%	2.92	29%	4.04	25%
Pillate	2.5	2.2	−0.18	2.23	1.99	−0.22	0.77	−0.51	17%	2.26	55%	4.27	27%
Punachizag	0.7	0.68	0.19	0.78	0.94	0.36	2.02	0.63	89%			3.67	11%
Quero	1.1	0.53	0.05	1.12	0.79	0.29	2.18	1	90%			3.72	10%
Retu	2.15	1.98	−0.11	2	1.97	−0.2	1.04	−1.21	19%	2.1	60%	3.97	21%
Saguazo	2.55	1.25	0.16	2.68	1.16	0.13	0.81	1.78	50%	2.8	23%	4.11	27%
San Pedro	2.6	1.58	−0.08	2.52	1.47	−0.12	0.84	0.7	28%	2.5	41%	4.01	31%
Santa Fe	2.75	1.45	−0.1	2.65	1.36	−0.16	0.88	1.29	35%	2.78	37%	4.1	28%
Santuario	2.65	1.73	−0.25	2.37	1.58	−0.27	0.97	0.04	18%	2.4	46%	3.83	35%
Yayulihui	1.1	1.33	0.58	1.62	1.3	0.58	1.08	0.87	74%	3.27	22%		
<i>Not affected by the 14th July eruption</i>													
Bayushig	2.15	0.4	0	2.15	0.54	0.21	1.84			2.1	93%		
Chogllontus 20-07	2.05	0.5	0.1	2.08	0.56	0.18	1.2			2.01	98%		
Chogllontus 24-07	2.25	0.8	0.19	2.35	0.86	0.17	1.25			2.14	86%	3.89	12%
El Altar	2	0.93	0.51	2.32	0.9	0.52	0.95			1.79	71%	3.5	26%
Ilapo	2.45	1.1	0.09	2.52	1.11	0.14	1.17			2.19	89%	4.63	11%
La Providencia	2.65	0.88	0.37	2.87	0.85	0.38	0.9			2.31	58%	3.69	39%
Matus Bajo	2.25	0.83	0.58	2.57	0.86	0.47	1.73			2.19	75%	3.83	20%
Palictahua	1.65	0.43	−0.06	1.63	0.65	0.19	2.16			1.58	89%	3.57	11%
Penipe	2.5	0.8	0.38	2.7	1.04	0.13	2.15			2.37	73%	3.98	18%
Puela	2.6	0.98	0.13	2.68	0.97	0.19	0.97			2.4	86%	4.21	14%
Pungal	2.95	0.88	0.49	3.23	0.84	0.46	0.99			2.73	65%	4.24	32%
San Andres	2.95	1.03	−0.02	2.93	1	0	0.94			2.97	100%		
TGSD	2.4	1.68	−0.07	2.32	1.57	−0.12	0.85	0.85	36%	2.59	38%	4.02	25%

and 2.73 ϕ and a secondary mode between 3.5 and 4.63 ϕ . The coarse mode is not found in these samples (Table 2), which is coherent with the fact that all are located in the SW sector. These results indicate that the coarse and the fine modes found in the samples from the global survey come mostly (for the coarse mode) or partially (for the fine mode) from the 14th July eruption. Based on this information, we propose to use a bimodal TGSD for the 14th July eruption with a coarse mode of 0.5 ϕ and a fine mode of 4 ϕ .

3.2. Componentry analysis and particle morphology

Componentry of the ash deposit was determined by a binocular microscope count at the Instituto Geofísico (EPN) using the Eychenne et al. (2013) method. Description and morphology analyses of the volcanic particles were done using Scanning Electron Microscope (SEM) and Morphology G3 instruments at the Laboratoire Magmas et Volcans (Blaise Pascal University, Clermont-Ferrand). The componentry for the 315–500 μm fraction of the 14th July sample is made up of 42 wt.% of free crystals (plagioclases and pyroxenes), 20 wt.% of dense black lithics, 14 wt.% of black scoriae, 12 wt.% of yellowish micro-vesiculated juveniles and up to 12 wt.% oxidized rocks (Fig. 5). The dense black lithics correspond to the degassed plug that was blown up by the vulcanian explosion. The presence of two types of vesiculated juveniles (black scoriae and yellowish micro-vesiculated juveniles) could indicate a volatile content or viscosity zonation of the magma in the conduit. The oxidized material and crystals are most likely associated to abrasion and fragmentation of the conduit wall rocks. The ash samples were prepared and analyzed using a protocol developed by Leibrandt and Le Pennec

(2015) and the morphology analyses for apparent 2-D projected images of the clasts in the 250–300 μm size range captured with a $\times 5$ optic yielded measurements of perimeter and area of each particle. The circularity of each grain is defined as the ratio of the perimeter of a disk whose area is equal to that of the grain over the measured irregular perimeter of the grain. For the studied clast population (>1000 grains) we obtained a mean circularity of 0.84 ± 0.07 , thus evidencing the fairly ragged morphology of the ash particles (Leibrandt and Le Pennec, 2015)

3.3. Plume height and mass eruption rate (MER)

According to the IGEPN, the 14th July 2013 eruption lasted from 06:47 to approximately 08:40 LT. However, the seismic-acoustic records show that the energetic phase occurred between 06:47 and 07:47 LT, i.e. lasted for one hour maximum. We estimate that most of the ash was emitted during this energetic phase. IGEPN reported a volcanic plume between 5 and 8.3 km above the volcano (avl). The advisory from the Washington VAAC indicated a first ash plume (06:51 LT) at 38,000 ft (~11.6 km asl or ~6.7 km avl) that rapidly divided into two clouds: one at 45,000 ft (~13.7 km asl or ~8.8 km avl) moving N and another at 32,000 ft (~9.7 km asl or ~4.8 km avl) moving E. Using the volume of emitted material and the duration of the high-energy phase, we estimated a volumetric discharge rate ranging between 28 and 39.5 m^3/s (Table 3). The highest cloud moved rapidly and was reported over Quito at 11:40 LT but without producing any ash fallout (IGEPN, 2013b). Measurements at the Runtun station (at the northern flank of the volcano) during the global survey also indicated that no significant fallout occurred in this region. Consequently, we interpret that the

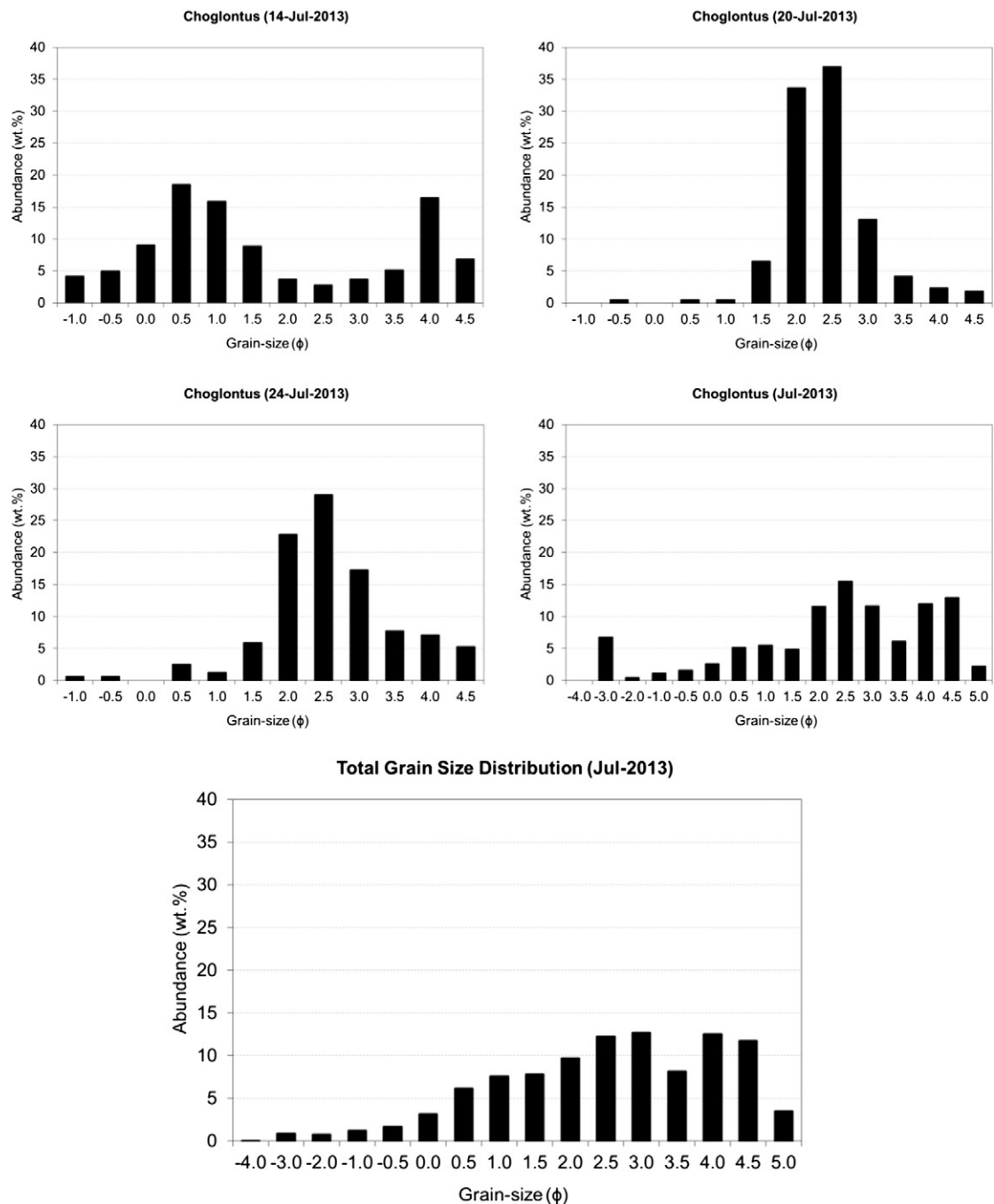


Fig. 4. Grain size histograms from the July 2013 eruption in weight %. Note the bimodal GSD of the 14th July sample. The 20th and 24th July samples have a different GSD with principal mode around 2ϕ . The Choglontus sample from the global survey and the TGSD have very similar histograms with trimodal distributions.

highest 8.8 km-high cloud moving N as gas and fine material produced during the first explosion occurred at 06:47 LT. In contrast, the plume associated to the high-energy tremor that lasted maximum one hour was probably at an altitude of about 5 km above the vent and produced ash fallout on the western side of the volcano.

4. Numerical simulations and fallout forecast

4.1. Model setup

The 14th July 2013 event was simulated coupling the Weather Research and Forecasting (WRF) model (Michalakes et al., 2004; WRF, 2015) with the FALL3D volcanic ash dispersion model (Costa et al., 2006; Folch et al., 2009).

WRF is a last-generation Eulerian non-hydrostatic model used for meteorological forecasting and weather research. It is a fully compressible model that solves the equations of atmospheric motion, with applicability to global, mesoscale, regional and local scales. We used the WRF (V3.2) model to generate the wind fields and other meteorological variables required later by FALL3D. The meteorological simulations used a master domain of 80×80 cells (each of 36×36 km) and two nested subdomains (Fig. 6), the second of which covers Ecuador with 199×199 cells (4 km horizontal resolution) and 35 vertical levels (model top pressure at 50 hPa, 22 km approximately). Initial and driving boundary conditions came from the NCEP FNL (Final) Operational Global Analysis data (NCEP, 2015). The meteorological simulation spanned from 13th July at 00:00 UTC (12th July at 19:00 LT) to 15th July at 23:00 UTC. It implies a model warm up of 36 h between the

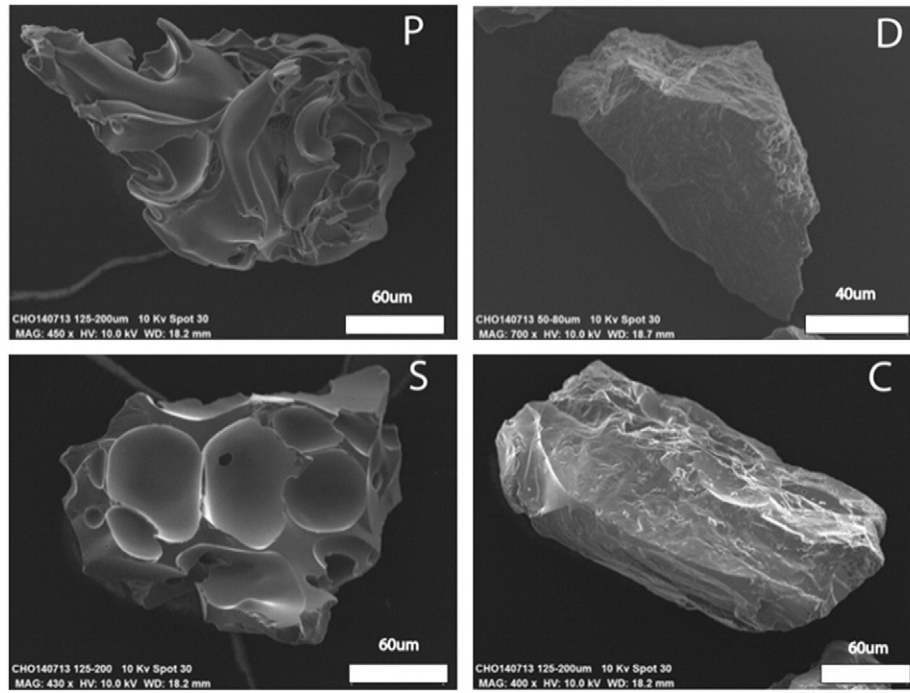


Fig. 5. SEM images of the componentry classes identified in the ash deposit. P: Yellowish micro-vesiculated juvenile; D: dense black lithic; S: scoria; C: free crystal. The oxidized particles cannot be distinguished from scoriae in SEM images.

beginning of the meteorological simulation and the start of the eruption (14th July at 12:00 UTC). WRF was configured using the following physical parameterizations (Skamarock et al., 2008): the double moment 6-class scheme for microphysics, the rapid radiative transfer model (rrtm) for long-wave radiation, the Duhdia scheme for short-wave radiation, the Monin–Obuknov scheme for the surface-layer option, the 5-layer thermal diffusion scheme for the land-surface option, and the Grell–Devenyi ensemble scheme for the cumulus option.

FALL3D is a 3D time-dependent Eulerian model for the transport and deposition of tephra. It solves the advection–diffusion–sedimentation equation on a structured terrain-following grid using a second-order finite-differences explicit scheme (Costa et al., 2006). We used

FALL3D-7.0 to model volcanic ash transport and sedimentation on a domain consistent with the inner WRF nest. The FALL3D domain has 199×199 cells with 20 km in height, divided in vertical layers of 500 m each.

According to the previous deposit analysis, the TGSD was taken as bi-Gaussian with two peak values of 0.5ϕ (0.71 mm) and 4ϕ (63 μm). We used the Suzuki (1983) source type with parameters $A = 5$, $L = 10$ (Pfeiffer et al., 2005), which concentrates mass at the column top in agreement with a vulcanian eruption. The eruption consisted of a column height of 8.80 km above the vent starting at 12:00 UTC (07:00 LT) and lasting 3 min followed by a second column of 4.85 km lasting 22 min. Three options were considered for modeling the horizontal turbulent

Table 3

Eruption parameters for the July–August 2013 eruption activity and for the 14th July paroxysm. (*) Maximum duration of the July 14th paroxysm that is most likely overestimated according to the seismo-acoustic record. (**) Calculated for 8.80 km-high eruptive column that is most likely overestimated.

July 2013					
Eruptive parameter	References/source	Equation/method	Minimum	Maximum	Average
Total Mass m_T ($\times 10^8$ kg)	Pyle (1989), Fierstein and Nathenson (1992) Legros (2000), Bonadonna and Costa (2012) Bernard, 2013	1 isomass; 1 segment; 2 segments; 3 segments; Weibull	6.26	7.20	6.72
Bulk density δ_B (kg m^{-3})		17 measurements	1094	1385	1255
Total Volume V_T ($\times 10^5$ m ³)		m_T/δ_B (average)	5.20	5.72	5.35
14th July 2013					
Eruptive parameters	References/source	Equation/method	Minimum	Maximum	Average
Percentage P	This study		40%	48%	44%
Mass M1 ($\times 10^8$ kg)		$m_T \times P$	2.50	3.46	2.96
Volume V ($\times 10^5$ m ³)		$V_T \times P$	2.08	2.75	2.35
Assumed magma density δ_{magma} (kg m^{-3})	Croweller et al. (2012)	Literature data/Andesite			2500
DRE1 volume ($\times 10^5$ m ³)		$M1 / \delta_{\text{magma}}$	1.00	1.38	1.18
Duration D (s)	IGEPN, this study		3600	6780(*)	
Column height H (km)	Washington VAAC (2014)		4.85	8.80	
Volumetric discharge rate Q1 ($\text{m}^3 \text{s}^{-1}$)		$DRE1 / D$ (3600)	28	38	33
MER1 ($\times 10^4$ kg s ⁻¹)		$M1 / D$	6.9	9.6	8.2
DRE2 volume ($\times 10^5$ m ³)	Mastin et al. (2009b)	$(H/2)^{(1/0.241)}$	1.42	16.84 (**)	
Volumetric discharge rate Q2 ($\text{m}^3 \text{s}^{-1}$)		$DRE2 / D$ (3600)	39.47	467.66 (***)	
MER2 ($\times 10^4$ kg s ⁻¹)		$Q2 \times \delta_{\text{magma}}$	9.47		
Mass M2 ($\times 10^8$ kg)		$MER2 \times D$ (3600)	3.41		

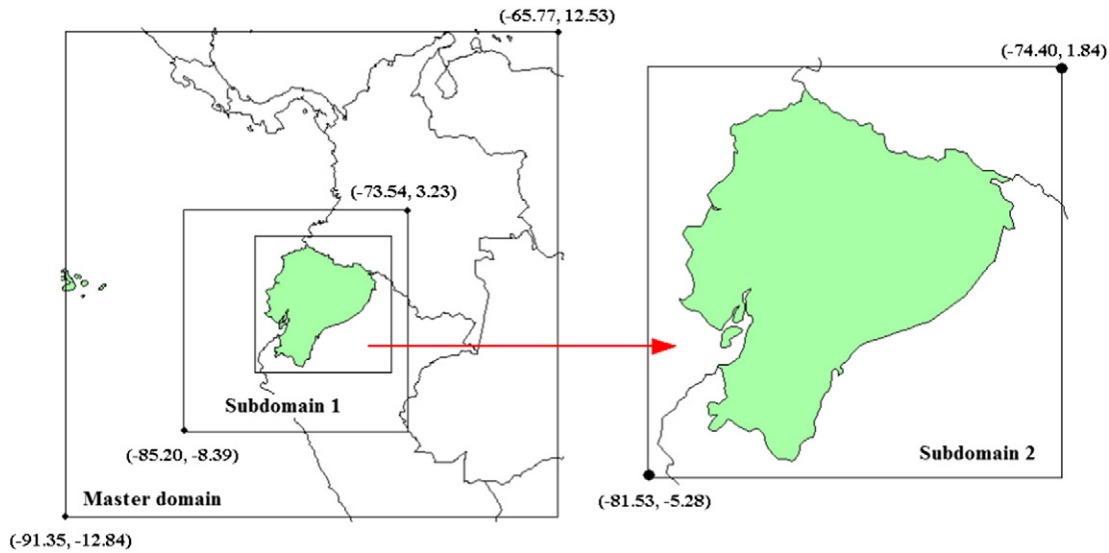


Fig. 6. Model simulation domains: master domain (80×80 cells, 36×36 km), subdomain 1 (109×109 cells, 12×12 km), subdomain 2 (199×199 cells, 4×4 km). Values are the geographical coordinates (longitude, latitude) of the corners.

diffusion: i) a constant value of $5000 \text{ m}^2/\text{s}$, ii) evaluated as in the Community Multiscale Air Quality (CMAQ) Modeling System (Byun and Schere, 2006) and, iii) evaluated as in the Regional Atmospheric Modeling System (RAMS) (Pielke et al., 1992).

We also did simulations using unique intermediate values for column height (e.g. 5.6 km). However, although fallout results were acceptable, the model was unable to reproduce the patterns of the ash clouds. In contrast, when using a column height of 8.8 km, the model did reproduce the ash clouds but overestimated fallout with respect to observations.

To estimate the mass flow rate we used the fit proposed by Mastin et al. (2009b). We also explored other options that consider the influence of wind on the plume (Degruyter and Bonadonna, 2012; Woodhouse et al., 2013). However, as opposed to other events (e.g. Mount St. Helens 1980 and Eyjafjallajökull 2010), these options provided mass flow values that overestimated the computed ash fall levels (between 1.7 and 4.5 times) in all the stations, in comparison with measurements.

4.2. Results

Table 4 compares ground ash load measurements with simulations at four stations for the three model turbulence options and gives the correlation coefficient (R^2) and the parameters “a” and “b” of the linear interpolation ($y = ax + b$; perfect fitting implies $R^2 = 1$, $a = 1$ and $b = 0$). Best results were found for the CMAQ option ($R^2 = 0.72$, $a = 0.67$, $b = 0.30$). The simulated deposit (Fig. 7) shows dominant ash fallout on the western side of Tungurahua, in agreement with the fallout reports (IGEPN, 2013b) and ground measurements. The simulated ash cloud patterns can be compared with the sketches provided by the Washington VAAC (2014) based on satellite imagery. The simulated clouds (Fig. 8) move mainly towards W, NW and N, in agreement with the behavior reported by the IGEPN (2013b) and with the sketches at different flight levels (FL).

4.3. Validation of the ESP

To validate the set of input ESP obtained from the 14th July event, we simulated two other eruptions from Tungurahua. The first started at 05:20 LT on 16th December 2012, producing a column of 2 km followed by three explosions that generated a column of 7 km at 06:02 LT (IGEPN, 2012). The dispersion pattern of this event was more variable compared

to that of 14th July 2013, given that wind direction varied between NNE and NNW causing fallout in the provinces of Tungurahua and Cotopaxi. The second started at 17:13 LT on 1st February 2014 forming a column of 3 km above the vent shortly followed by two larger eruptions (at 17:22 and 17:39) producing a column of 8 km (IGEPN, 2014). The wind direction was mainly towards S and ash fallout affected the provinces of Chimborazo, Cañar, Bolivar and Azuay (IGEPN, 2014). It is clear that the actual ESP (mainly duration and column height) differ from the pre-defined ones but, nonetheless, modeled values still show a relatively good correlation with measurements (Table 5). Although with certain differences, results are consistent with observations, showing higher modeled values at stations with higher observed records. In terms of ash clouds, differences exist for the December 2012 eruption (Fig. 9) whereas for the February 2014 eruption results are in better agreement with the Washington VAAC sketches (Fig. 10). For the three eruptions, modeled results of volcanic ash fall were consistent with the corresponding measurements (Fig. 11).

For these eruptions we also did simulations using reported information of time and column height for each one (12-Dec-2012; 2 km / 40 min + 7 km / 5 min) (01-Feb-2014, 3 km / 15 min + 8 km / 15 min). The computed ground load values and the fitting parameters improved (Fig. 11, Table 5).

5. Discussion and summary

The ESP for Tungurahua volcano derived in this paper are an improvement with respect to the previous values, based on an eruption

Table 4
Comparison between measured and modeled deposit load at four different locations for the 14th July 2013 event. (*) Expected range.

Station	Measured	Modeled results		
		Horizontal turbulence diffusion		
		Constant	CMAQ	RAMS
Choglontus (kg m^{-2})	1.206	0.793	1.046	0.810
Palictahua (kg m^{-2})	0.000	0.411	0.393	0.412
Pilllate (kg m^{-2})	0.304	0.612	0.770	0.623
Runtun (kg m^{-2})	0.019	0.047	0.020	0.045
R^2		0.63	0.72	0.64
Parameter a (perfect fitting = 1)		0.45	0.67	0.46
Parameter b (perfect fitting = 0)		0.29	0.30	0.30
Erupted mass ($\times 10^8 \text{ kg}$)	2.5–3.41(*)	3.27		

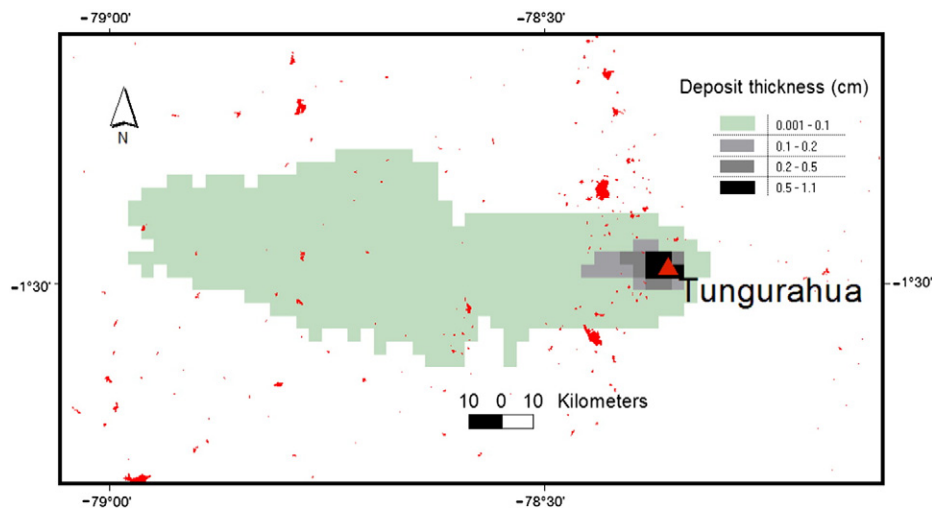


Fig. 7. Simulated deposit thickness (cm) for 14th Jul 2013 at 18:00 LT using the CMAQ option for horizontal turbulent diffusion.

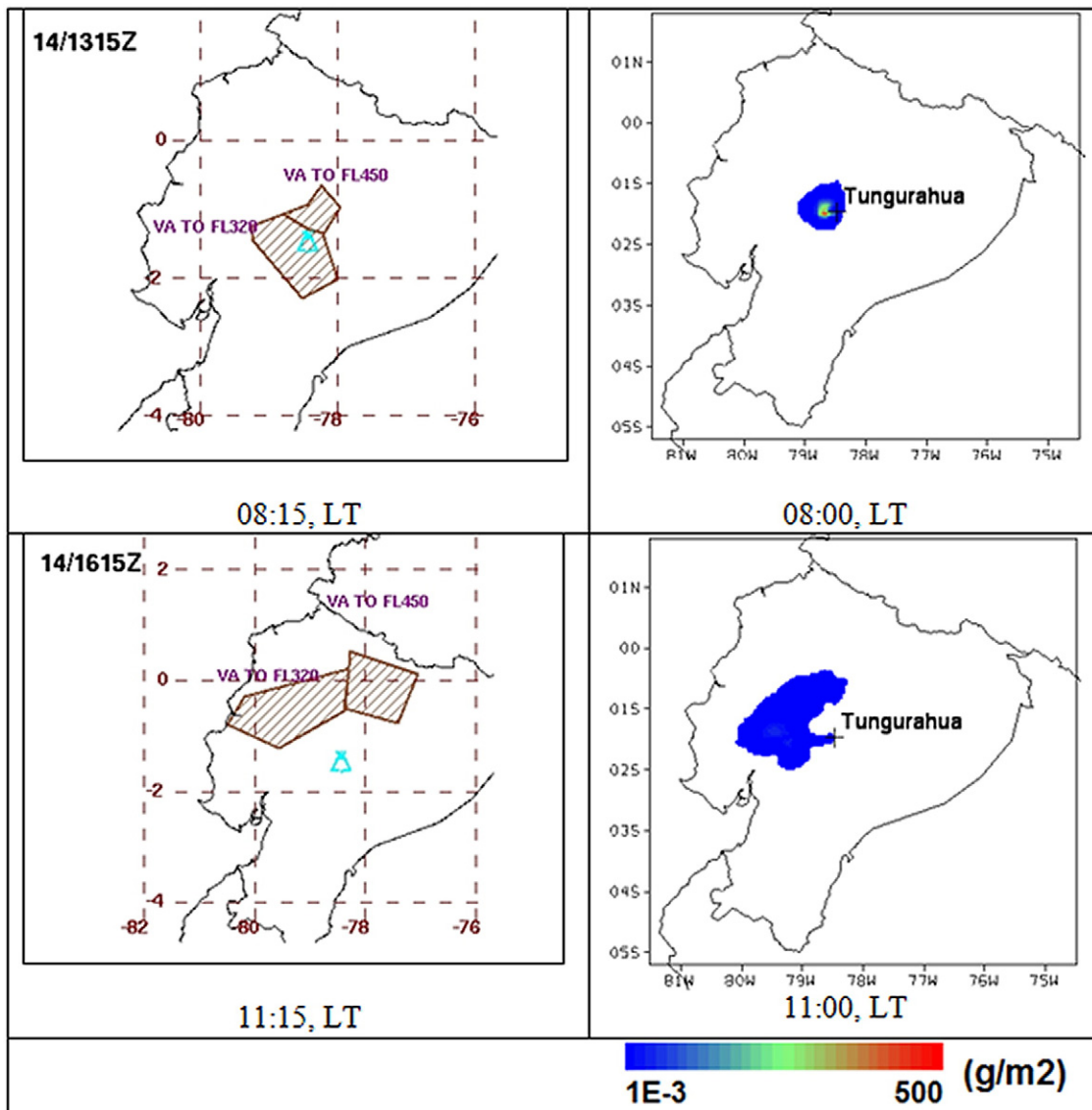


Fig. 8. Washington VAAC's sketches (left) versus simulated (CMAQ option for horizontal turbulent diffusion) ash cloud column mass (in g/m^2) (right) on Jul 14th 2013.

Table 5
Comparison between observed and modeled ground load: (a) using pre-defined ESP, (b) using reported information of time and column height for each eruption.

Station	16th Dec 2012			1st Feb 2014		
	Measurement	Modeled (a)	Modeled (b)	Measurement	Modeled (a)	Modeled (b)
Choglontus (kg m^{-2})	0.000	0.076	0.008	0.144	0.246	0.522
Palictahua (kg m^{-2})	0.000	0.017	0.004	1.420	0.536	1.089
Pillate (kg m^{-2})	0.000	0.103	0.020	0.067	0.047	0.092
Runtun (kg m^{-2})	0.472	0.827	0.366	0.013	0.016	0.027
R ²		0.99	1		0.87	0.86
Parameter a (perfect fitting = 1)		1.61	0.75		0.33	0.67
Parameter b (perfect fitting = 0)		0.07	0.01		0.08	0.16

of type S2 as defined by Mastin et al. (2009a). The main updated parameters are duration, mass eruption rate and mass fraction of erupted material smaller than $63 \mu\text{m}$ (Table 6). Regarding column height, Mastin et al. (2009a) assign a value of 5 km, which is comparable with the lower value considered here (4.85–8.8 km). During the eruption of 14th July 2013, the higher ash cloud was likely formed by dispersion of gas and fine material released at about 8.8 km (3 min of duration for modeling), whereas fallout came from particles emitted at a shorter height (4.85 km), but during a larger time interval (22 min for modeling).

With these pre-defined ESP we also did simulations using domains of 1 km of spatial resolution, both for the meteorological and ash dispersion components. However the results did not improved significantly in comparison with the results obtained using the domains of 4 km.

We have defined a set of ESP for modeling ash dispersion and fallout from vulcanian eruptions at Tungurahua volcano based on the July 14th 2013 eruption and using state-of-the-art models, high-quality deposit data and ash cloud patterns from the Washington VAAC. The parameters have been later used to simulate ash fallout from eruptions occurring on 16th Dec 2012 and 1st Feb 2014, assuming that no other

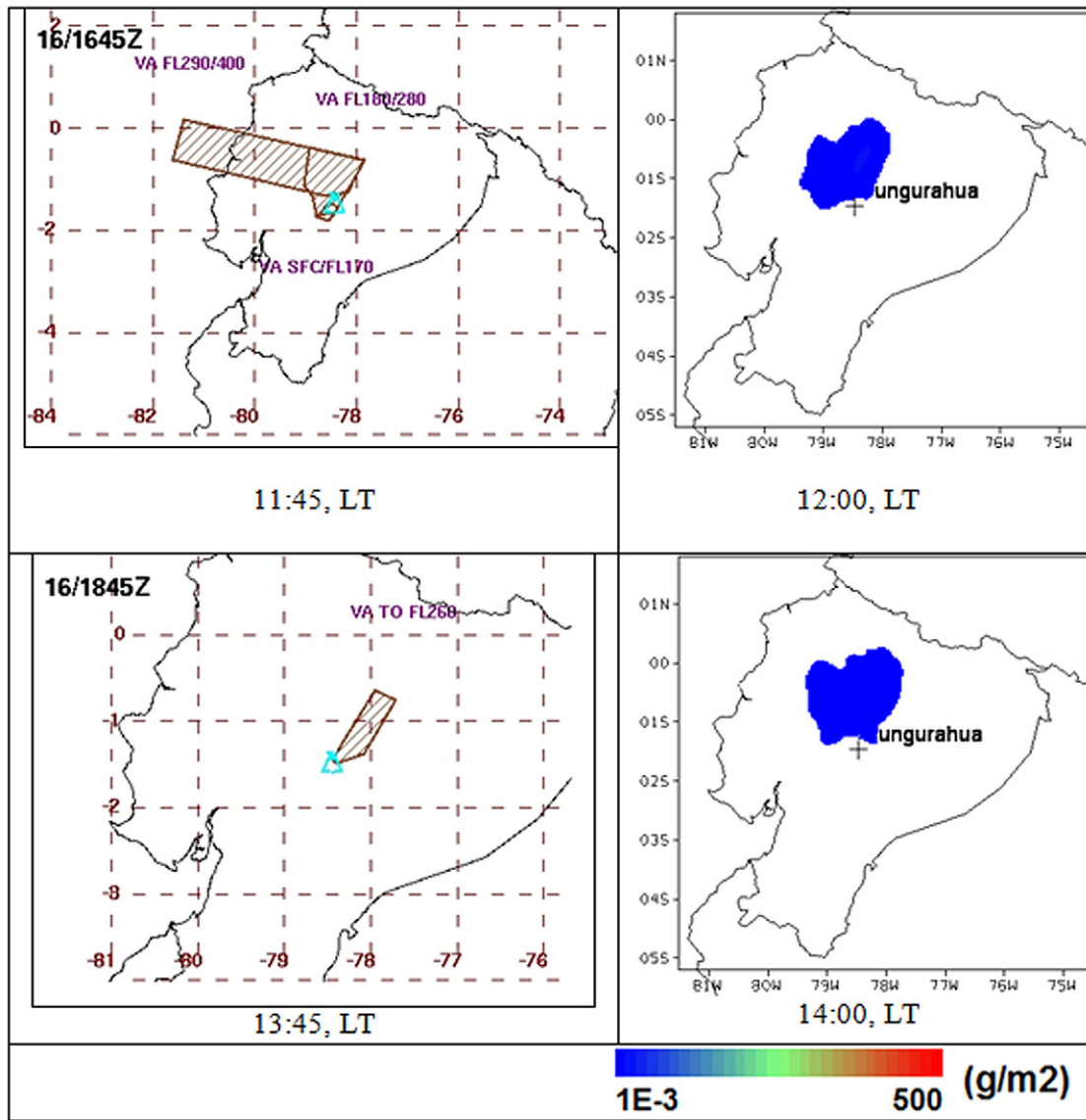


Fig. 9. Washington VAAC's sketches (left) versus simulated cloud column mass (in g/m^2) (right) on Dec 16th 2012.

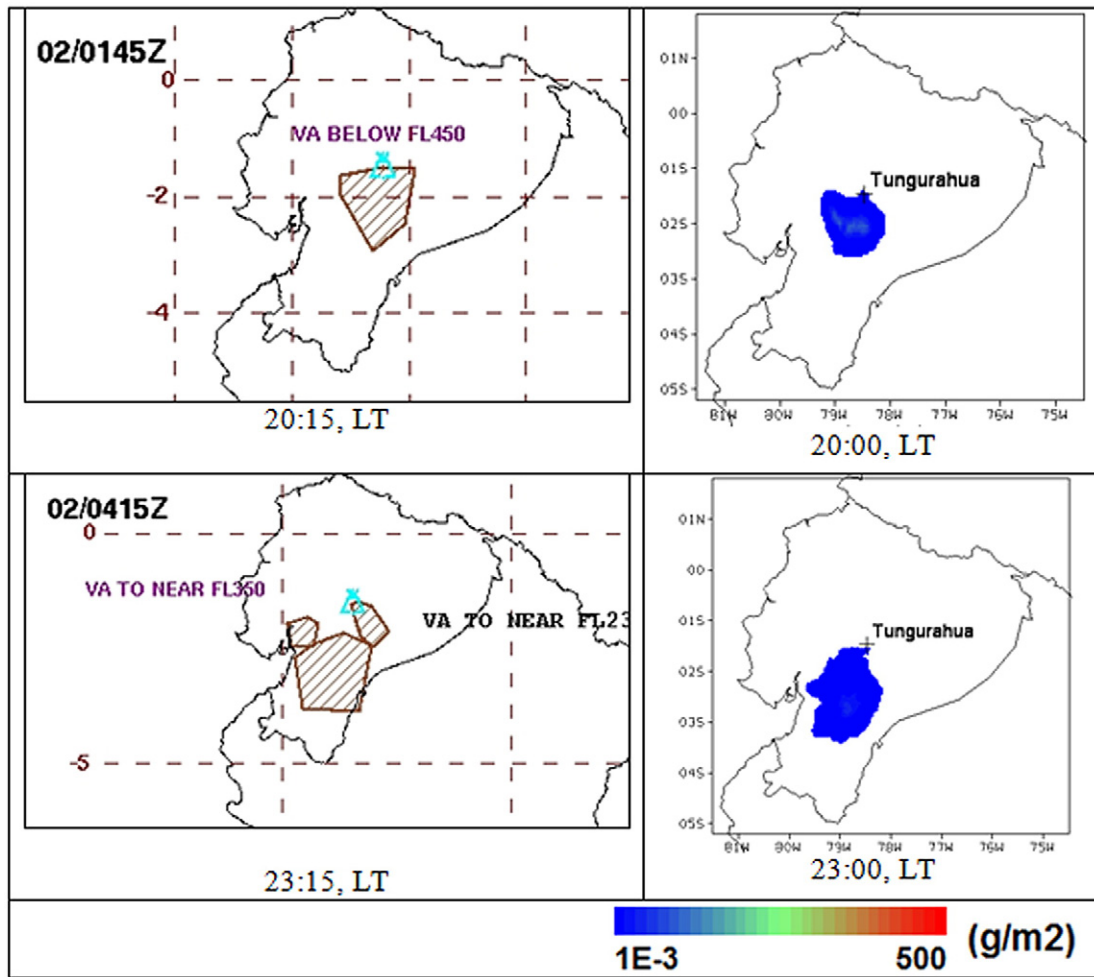


Fig. 10. Washington VAAC's sketches (left) versus simulated cloud column mass (in g/m^2) (right) on Feb 1st 2014.

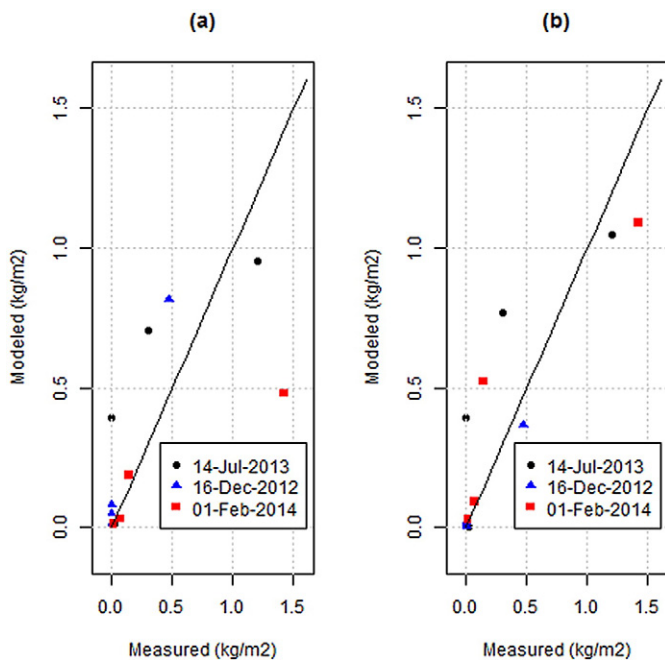


Fig. 11. Comparison of measurements and modeled results for ash fallout from Tungurahua: 14-Jul-2013 used in the calibration phase, (a) 12-Dec-2012 and 01-Feb-2014 used for validation with the pre-defined ESP, (b) obtained with reported information of time and height for each eruption occurring on 12-Dec-2012 and 01-Feb-2014.

inputs are available (except the eruption starting time). Modeling results are consistent both for ash cloud patterns and fallout. The WRF model generated congruent wind fields in height, as relevant data for volcanic ash dispersion. Based on the results, we propose the following set of ESP for forecasting ash dispersion from vulcanian eruptions at Tungurahua volcano, when no observations are available (or shortly before the eruption):

- 1 Height above the vent: 8.80 km during 3 min, followed by column height of 4.85 km during 22 min.
- 2 Estimation of the mass flow rate according to Mastin et al. (2009b).
- 3 Source type: Suzuki (1983) with $A = 5$ and $L = 10$.
- 4 TGSD: bi-Gaussian distribution (mean σ values of 4 and 0.5).
- 5 Circularity range: 0.77–0.91.
- 6 Scheme for horizontal turbulence (FALL3D model): CMAQ.

Table 6
Comparison of the ESP defined for vulcanian eruptions of the Tungurahua versus the ESP assigned by Mastin et al. (2009a).

Parameter	This paper	Mastin et al (2009a)
Height above the vent (km)	4.85 (22 min)–8.80 (3 min)	5.00
Duration (h)	0.42	12
Mass eruption rate (kg s^{-1})	0.95×10^5 (22 min)– 11.2×10^5 (3 min)	2×10^5
Erupted volume (km^3)	0.0002	0.003
Mass fraction of erupted tephra smaller than $63 \mu\text{m}$	0.153	0.10

Using these ESP and the domains presented in this paper, the GIVCE simulate daily ash dispersion and deposition at Tungurahua volcano, assuming a scenario similar to the 14th July 2013 eruption. Meteorological fields are forecasted for 3 days. Results of the inner subdomain are used to simulate the ash behavior during the second and third days. The dedicated computational resources are 24 cores (2.00 GHz, 24 GB RAM) which requires about 25 h, corresponding 80% to the meteorological component.

These simulations can become handy, especially when no observations are available or cloudiness does not allow satellite tracking of ash plumes. Such a situation is highly probable in the Andean region of Ecuador, where convective wet air masses, as those coming from the coast and the Amazon regions or by the presence of the Intertropical Convergence Zone, typically promote the formation of clouds (Krishnamurti et al., 2013), (Gadgil and Guruprasad, 1990).

The ESP presented in this paper and the operational forecasting of ash dispersion and fallout for vulcanian eruptions from the Tungurahua volcano, are important milestones for the objectives of the GIVCE, and produce expectancy for future inclusion of other active volcanoes in Ecuador, as El Reventador, Sangay, Pichincha and Cotopaxi.

Acknowledgments

The fieldwork to collect ash samples was funded by a USFQ Chancellor Grant (Bernard 2013 n°13). This research is part of the project “Grupo de Investigación sobre la Ceniza Volcánica en Ecuador” funded with a USFQ Collaboration Grant 2014 (Bernard and Parra 2014). The authors thank the Instituto Geofísico de la Escuela Politécnica Nacional (Quito, Ecuador) for logistical assistance in the field and providing access to the binocular microscope. In particular we thank Silvana Hidalgo. The authors thank the Laboratoire Magmas et Volcans of the Université Blaise Pascal (Clermont-Ferrand, France) for the access to the SEM and the Morphology 3G instruments, in particular Sébastien Leibrandt. We thank also to John Skukalek who checked the English grammar. Simulations were performed at the High Performance Computing system at the USFQ.

Appendix A. Supplementary data

Supplementary data to this article can be found online at <http://dx.doi.org/10.1016/j.jvolgeores.2015.11.001>.

References

- Ayris, P.M., Delmelle, P., 2012. The immediate environmental effects of tephra emission. *Bull. Volcanol.* 74, 1905–1936. <http://dx.doi.org/10.1007/s00445-012-0654-5>.
- Bernard, B., 2013. Homemade ashmeter: a low-cost, high-efficiency solution to improve tephra field-data collection for contemporary explosive eruptions. *J. Appl. Volcanol.* 2–1. <http://dx.doi.org/10.1186/2191-5040-2-1>.
- Bernard, B., Bustillos, J., Ramon, P., Vallejo, S., 2012. Near real-time data collection during tephra fallout: a new monitoring system at Tungurahua volcano. Abstract of the 7th Cities on Volcanoes Conference, November 19–23, Colima (Mexico), Session 2.2.
- Bernard, B., Bustillos, J., Wade, B., Hidalgo, S., 2013a. Influence of the wind direction variability on the quantification of tephra fallouts: December 2012 and March 2013 Tungurahua eruptions. *Av. Cienc. Ing.* 5–1, A14–A21.
- Bernard, B., Wade, B., Hidalgo, S., Bustillos, J., 2013b. Quantification of tephra deposits from Tungurahua 2011–2013 eruption, Ecuador: implication on the evolution of a long-lasting eruption. IAVCEI Scientific Assembly, July 20–24, Kagoshima (Japan), session 3 F, poster P8.
- Bonadonna, C., Costa, A., 2012. Estimating the volume of tephra deposits: a new simple strategy. *Geology* 40–5, 415–418. <http://dx.doi.org/10.1130/G32769.1>.
- Bonadonna, C., Houghton, B.F., 2005. Total grain-size distribution and volume of tephra fall deposits. *Bull. Volcanol.* 67, 441–456. <http://dx.doi.org/10.1007/s00445-004-0386-2>.
- Bonadonna, C., Folch, A., Loughlin, S., Puempel, H., 2011. Future developments in modeling and monitoring of volcanic ash clouds: outcomes from the first IAVCEI-WMO workshop on ash dispersal forecast and civil aviation. *Bull. Volcanol.* <http://dx.doi.org/10.1007/s00445-011-0508-6>.
- Bonasia, R., Scaini, C., Capra, L., Nathenson, M., Siebe, C., Arana-Salinas, L., Folch, A., 2014. Long-range hazard assessment of volcanic ash dispersal for a Plinian eruptive scenario at Popocatepetl volcano (Mexico): implications for civil aviation safety. *Bull. Volcanol.* 76 (789). <http://dx.doi.org/10.1007/s00445-013-0789-z>.
- Byun, D., Schere, K., 2006. Review of the governing equations, computational algorithm and other components of the Model-3 Community Multiscale Air Quality (CMAQ) modeling system. *Appl. Mech. Rev.* 59, 51–77.
- Collini, E., Osorio, M.S., Folch, A., Viramonte, J., Villarosa, G., Salmuni, G., 2013. Volcanic ash forecast during the June 2011 Condón Caille eruption. *Nat. Hazards* 6 (2), 389–412. <http://dx.doi.org/10.1007/s11069-012-0492-y>.
- Costa, A., Macedonio, G., Folch, A., 2006. A three dimensional Eulerian model for transport and deposition of volcanic ash. *Earth Planet. Sci. Lett.* 241, 634–647.
- Croswell, H.S., Arora, B., Brown, S.K., Cottrell, E., Deline, N.L., Guerrero, N.O., Hobbs, L., Kiyosugi, K., Loughlin, S.C., Lowndes, J., Nayemil, M., Siebert, L., Sparks, R.S.J., Takarada, S., Venzke, E., 2012. Global database on large magnitude explosive volcanic eruptions (LaMEVE). *J. Appl. Volcanol.* 1, 4. <http://dx.doi.org/10.1186/2191-5040-1-4>.
- Degruyter, W., Bonadonna, C., 2012. Improving on mass flow rate estimates of volcanic eruptions. *Geophys. Res. Lett.* 39, L16308. <http://dx.doi.org/10.1029/2012GL052566>.
- Eychenne, J., Le Pennec, J.L., Troncoso, L., Gouhier, M., Nedelec, J., 2012. Causes and consequences of bimodal grain-size distribution of tephra fall deposited during the August 2006 Tungurahua eruption (Ecuador). *Bull. Volcanol.* 74–1, 187–205. <http://dx.doi.org/10.1007/s00445-011-0517-5>.
- Eychenne, J., Le Pennec, J.L., Ramón, P., Yepes, H., 2013. Dynamics of explosive paroxysms at open-vent andesitic systems: high-resolution mass distribution analyses of the 2006 Tungurahua fall deposit (Ecuador). *Earth Planet. Sci. Lett.* 361, 343–355. <http://dx.doi.org/10.1016/j.epsl.2012.11.002>.
- Fierstein, J., Nathenson, M., 1992. Another look at the calculation of fallout tephra volumes. *Bull. Volcanol.* 54, 156–167.
- Folch, A., Jorba, O., Viramonte, J., 2008. Volcanic ash forecast – application to the May 2008 Chaitén eruption. *Nat. Hazards Earth Syst. Sci.* 8, 927–940. <http://dx.doi.org/10.5194/nhess-8-927-2008>.
- Folch, A., Costa, A., Macedonio, G., 2009. FALL3D: a computational model for transport and deposition of volcanic ash. *Comput. Geosci.* 35 (6), 1334–1342.
- Gadgil, S., Guruprasad, A., 1990. An objective method for the identification of the Intertropical Convergence Zone. *J. Clim.* 3, 558–567.
- Hall, M.L., Robin, C., Beate, B., Mothes, P., Monzier, M., 1999. Tungurahua volcano, Ecuador: structure, eruptive history and hazards. *J. Volcanol. Geotherm. Res.* 91 (1), 1–21.
- Heiken, G., Wohletz, K., 1985. *Volcanic Ash*. University of California Press, California (245 pp.).
- Hidalgo, S., Battaglia, J., Arellano, S., Steele, A., Bernard, B., Bourquin, J., Galle, B., Arrais, S., Vásquez, F., 2015. SO₂ degassing at Tungurahua volcano (Ecuador) between 2007 and 2013: transition from continuous to episodic activity. *J. Volcanol. Geotherm. Res.* 298, 1–14. <http://dx.doi.org/10.1016/j.jvolgeores.2015.03.022>.
- Horwell, C.J., Baxter, P.J., 2006. The respiratory health hazards of volcanic ash: a review for volcanic risk mitigation. *Bull. Volcanol.* 69 (1), 1–24.
- IGEPN, 2012. Informe Especial del Volcán Tungurahua No. 10, Instituto Geofísico, Escuela Politécnica Nacional. <http://www.igepn.edu.ec/> (Accessed 9 April 2014).
- IGEPN, 2013a. Informe del Estado del Volcán Tungurahua No. 195, Instituto Geofísico, Escuela Politécnica Nacional. <http://www.igepn.edu.ec/> (Accessed 9 April 2014).
- IGEPN, 2013b. Informe especial del Volcán Tungurahua No. 14, Instituto Geofísico, Escuela Politécnica Nacional. <http://www.igepn.edu.ec/> (Accessed 9 April 2014).
- IGEPN, 2014. Informe del Estado del Volcán Tungurahua No. 33, Instituto Geofísico, Escuela Politécnica Nacional. <http://www.igepn.edu.ec/> (Accessed 9 April 2014).
- Kim, K., Lees, J.M., Ruiz, M.C., 2014. Source mechanism of vulcanian eruption at Tungurahua volcano, Ecuador, derived from seismic moment tensor inversions. *J. Geophys. Res. Solid Earth* 119. <http://dx.doi.org/10.1002/2013JB010590>.
- Krishnamurti, T., Stefanova, L., Misra, V., 2013. The Intertropical Convergence Zone. *Tropical Meteorology – An Introduction*. Springer Atmospheric Sciences http://dx.doi.org/10.1007/978-1-4614-7409-8_3.
- Kueppers, U., Putz, C., Spieler, O., Dingwell, D.B., 2012. Abrasion in pyroclastic density currents: insights from tumbling experiments. *Phys. Chem. Earth A* 45–46, 33–39. <http://dx.doi.org/10.1016/j.pce.2011.09.002>.
- Le Pennec, J.L., Ruiz, G.A., Ramón, P., Palacios, E., Mothes, P., Yepes, H., 2012. Impact of tephra falls on the Andean communities: the influences of eruption size and weather conditions during the 1999–2001 activity of Tungurahua volcano, Ecuador. *J. Volcanol. Geotherm. Res.* 217–218, 91–103. <http://dx.doi.org/10.1016/j.jvolgeores.2011.06.011>.
- Legros, F., 2000. Minimum volume of a tephra fallout deposit estimated from a single isopach. *J. Volcanol. Geotherm. Res.* 96, 25–32.
- Leibrandt, S., Le Pennec, J.L., 2015. Towards fast and routine analyses of volcanic ash morphology for eruption surveillance applications. *J. Volcanol. Geotherm. Res.* 297, 11–27. <http://dx.doi.org/10.1016/j.jvolgeores.2015.03.014>.
- Macedonio, G., Costa, A., Longo, A., 2005. A computer model for volcanic ash fallout and assessment of subsequent hazard. *Comput. Geosci.* 31, 837–845.
- Mastin, L.G., Guffani, M., Servranckx, R., Webley, P., Barsotti, S., Dean, K., Durant, A., Ewert, J.W., Neri, A., Rose, W.L., Schneider, D., Siebert, L., Stunder, B., Swanson, G., Tupper, A., Volentik, A., Waythomas, C.F., 2009a. A multidisciplinary effort to assign realistic source parameters to models of volcanic ash-cloud transport and dispersion during eruptions. *J. Volcanol. Geotherm. Res.* 186, 10–21.
- Mastin, L.G., Guffani, M., Ewert, J.W., Spiegel, J., 2009b. Preliminary spreadsheet of eruption source parameters for volcanoes of the world. U.S. Geological Survey Open-file Report 2009-1133, v. 1.2 (25 p.).
- Michalakes, J., Dudhia, J., Gill, D., Henderson, T., Klemp, J., Skamarock, W., Wang, W., 2004. The weather research and forecast model: software architecture and performance. In: Zwiefelhofer, Walter, Mozdzyński, George (Eds.), *Proc. of the Eleventh ECMWF Workshop on the Use of High Performance Computing in Meteorology*. World Scientific, pp. 156–168.
- NCEP, 2015. NCEP FNL Operational Model Global Tropospheric Analyses, continuing from July 1999, Research data archive at the National Center for Atmospheric Research,

- Computational and Information Systems Laboratory. <http://rda.ucar.edu/datasets/ds083.2> (Accessed 31 March 2015).
- Pfeiffer, T., Costa, A., Macedonio, G., 2005. A model for the numerical simulation of tephra fall deposits. *J. Volcanol. Geotherm. Res.* 140, 273–294.
- Pielke, R., Cotton, W., Walko, R., Tremback, C., Lyons, W., Grasso, L., Nicholls, M., Moran, M., Wesley, D., Lee, T., Copeland, J., 1992. A comprehensive meteorological modeling system – RAMS. *Meteorog. Atmos. Phys.* 49, 69–91.
- Pyle, D., 1989. The thickness, volume and grain size of tephra fall deposits. *Bull. Volcanol.* 51, 1–15. <http://dx.doi.org/10.1007/BF0108675>.
- Scollo, S., Prestifilippo, M., Spata, G., D'Agostino, M., Coltelli, M., 2009. Monitoring and forecasting Etna volcanic plumes. *Nat. Hazards Earth Syst. Sci.* 9, 1573–1585.
- Self, S., Wilson, L., Nairn, L., 1979. Vulcanian eruption mechanisms. *Nature* 277, 440–443.
- Skamarock, W., Klemp, J., Dudhia, J., Barker, D., Duda, M., Huang, X., Wang, W., Powers, J., 2008. A description of the advanced research WRF version 3. NCAR/TN-475 + STR. NCAR Technical Note. Mesoscale and Microscale Meteorology Division. National Center for Atmospheric Research, Boulder, USA.
- Suzuki, T., 1983. A theoretical model for dispersion of tephra. In: Shimozuru, D., Yokoyama, I. (Eds.), *Arc Volcanism: Physics and Tectonics*. Terrapub, pp. 95–113.
- Washington VAAC, 2014. Washington DC Volcanic Ash Advisory Center. www.ssd.noaa.gov/VAAC/washington.html (Accessed 31 Mar 2014).
- Wilkins, K., Watson, M., Webster, H., Thomson, D., Dacre, H., Mackie, S., Harvey, N., 2014. Volcanic ash cloud forecasting: combining satellite observations and dispersion modelling. *Geophys. Res. Abstr.* 16 (EGU2014-1615).
- Wilson, T.M., Stewart, C., 2012. Volcanic ash. In: Bobrowsky, P. (Ed.), *Encyclopedia of Natural Hazards*. Springer, p. 1000.
- Wohletz, K., Sheridan, M., Brown, W., 1989. Particle size distributions and the sequential fragmentation/transport theory applied to volcanic ash. *J. Geophys. Res.* 94 (15), 15703–15721.
- Woodhouse, M., Hogg, A., Phillips, J., Sparks, R., 2013. Interactions between volcanic plumes and winds during the 2010 Eyjafjallajökull eruption, Iceland. *J. Geophys. Res. Solid Earth* 118, 92–109. <http://dx.doi.org/10.1029/2012JB009592>.
- WRF, 2015. The Weather Research & Forecasting Model. <http://www.wrf-model.org/index.php> (Accessed 31 Mar 2015).